Supplementary Materials for 'The emergence of top-down controls on marine biomass in the 21st century'

Tyler Rohr,[1,2*]

*To whom correspondence should be addressed; E-mail: tyler.rohr@utas.edu.au.

This PDF Includes

Supplementary Text 1

Supplementary Figures 1-12

1 Dummy Section

Supplementary Text 1: Detailed Description of Case Studies

Detailed descriptions of all case studies presented in Supplementary Figures 7-9 are provided below. This includes expanded analysis/figures of all case studies from Fig 6. Regional boundaries were selected for illustrative purposes by filtering for increasing/decreasing biomass under bottom-up/top-down control within a specified Longhurst province. Colormaps are as per Fig. 2.

Sub-panels in the first 4 columns show the $\overline{2010-2015}$ (dashed) and $\overline{2095-2100}$ (solid) climatologies for specified variables. Arrows and shading indicate the direction of change. In all sub-panels, the mean-annual relative change in each property ($\Delta_{\%}$) is annotated. In all Supplementary Figures, sub-panels are provided for the climatological change in physics (*i*, *vi*), specific biological rates (*ii*, *vii*) and depth-integrated biomass (*iii*, *viii*). The sub-panels in the second rightmost column (fourth) vary between case studies and are selected to illustrate how/why loss rates are evolving in a particular way. In some cases a profile is included or inset, in which case the month the profile was sampled from is annotated. Boarders are color-coated to reflect the pathway they help explain. See 'Methods' for descriptions of all plotted diagnostics.

In the rightmost row for each Supplementary Figure is a decomposition of the drivers of changing loss rates (Δl; 'see Methods'). Non-grazing terms are plotted as dashed lines in *v* and with lighter shading in *x*. In sub-panel *v*, timeseries of Δl_i show the climatological contribution of each of each driver to the changes in Δl_g and Δl_{ng} plotted in sub-panel *vii*. In sub-panel *x*, the mean-annual magnitude share (see 'Methods') of each driver's contribution is time-average and biomass-weighted as to not inflate the influence of large contributions during periods of negligible biomass. Grazing and non-grazing contributions are stacked and protrude outward (inwards) from the inner circle is their contribution is positive (negative).

1.1 CMOC - Southern Ocean

In CMOC, the Southern Ocean experiences a widespread increase in biomass, which is clearly driven from the bottom-up (Supplementary Fig. 7a). The combination of a relatively small MLD shoaling (panel *i*) and large SST increase (*vi*) allow light and temperature to drive phytoplankton division rates up (*ii*) up by 18%, dominating any influence of restricted nutrient access. Improved growth conditions translate to a 31% increase depth-integrated phytoplankton biomass throughout the year (*iii*). Non-grazing (l_{ng}) and grazing (l_g) pressure follow and increase (*vii*) by 5% and 29%, respectively. The increase in l_{ng} is dominated by the contribution of changes in phytoplankton biomass ($\Delta l_{ng,\Sigma P}$ *v,x*, dashed green), which is driven by the non-linear (concave upward) quadratic loss term operating on an elevated mean biomass-weighted phytoplankton concentration (*iv*). Alternatively, the increase in l_g is dominated by the contribution of changes in zooplankton biomass ($\Delta l_{ng,\Sigma Z}$ *v,x*, purple) which increases by 30% (*viii*). Clearance rates also increase by 8% (not shown), reflecting the increased grazing efficiency of individual zooplankton on larger prey concentrations (*iv*). Collectively, this is a typical negative feedback in predator-prey dynamics through which the increasing prey population supports a larger, more efficient predator population, which buffers the original bottom-up driven changes in the prey abundance.

Note, however, the stabilizing feedback of increasing phytoplankton biomass on loss rates ($l_{\Sigma P}$) is felt primarily through the non-grazing contribution ($l_{ng,\Sigma P}$; *v,x*, dashed green), rather than the grazing contribution ($l_{g,\Sigma P}$). This occurs because of the large quadratic non-grazing mortality term (Supplementary Fig. 4b). Alternately, the influence of increasing prey biomass on grazing efficiency (ie. clearances rates) is small due to the competing effect of increasing and decreasing clearance rates at different depths ($l_{g,\Sigma P}$; *v, x*, green). This occurs because CMOC uses a sigmoidal response function for grazing parameterized with a relatively small $K_{1/2}$. In a sigmoidal response curve, clearance rates increase as prey concentrations increase

below $K_{1/2}$ but decrease as prey concentrations increase above $K_{1/2}$ decreases. In turn, biomass gains above $K_{1/2}$ near the surface but below $K_{1/2}$ at depth (*ix*) largely cancel out in terms of depth-integrated, biomass-weighted grazing efficiency. Combined with models which prescribe a consistently downwardly concave type II grazing response (iHAMMOCC, MARBL, CanOE), this explains why $\Delta l_{g,\Sigma P}$ is destabilizing ($\frac{\Delta l_{\Sigma P}}{\Sigma P} < 0$) for 37$\%$ of ensemble biomass (Supplementary Fig. 10a)

Regarding other loss rate drivers, the influence of changes in the vertical distribution (Δl_{VD}; *v, x*, blue) is small due to small changes in the dilution length scale ($\Delta_{\%} l_{VD} = -2\%$; not shown) associated with small changes in the MLD. There is no influence of temperature on loss rates because there are no temperature dependencies on any grazing or non-grazing loss terms and there is no influence from community composition because only one group of phytoplankton and one group of zooplankton are resolved (Supplementary Fig. 4). Finally, interaction effects (*v, x*), black) play very little role, further confirming the response is dominated by bottom-up feedbacks on phytoplankton and zooplankton biomass.

1.2 MEDUSA2.1 - Southern Ocean

Similarly, in MEDUSA2.1, the Southern Ocean experiences a widespread increase in biomass driven from the bottom-up (Supplementary Fig. 7b), but now it is amplified from the top-down by changes in community composition. From the bottom-up, MLD shoaling (*i*) and SST increase (*vi*) combine to relieve light and temperature limitation and drive phytoplankton division rates up (*ii*) by 23$\%$. Improved growth conditions again translate to elevated phytoplankton biomass throughout the year (*iii*), followed by elevated zooplankton biomass (*viii*) and loss rates (*vii*). Similar to CMOC, the change in grazing pressure (l_g) is dominated by an increase in the amount of grazers (*v, x*, purple) rather than an increase in their grazing efficiency (*v, x*, green).

On the other hand, unlike in CMOC, there is very little amplification of loss rates through non-grazing processes due to the absence of quadratic mortality term. Instead, during the summer, a shift in community composition from smaller to larger species (*iv, ix*) works to buffer the increase in grazing pressure (*v, x*, teal) and thus amplifies the increase in biomass. Note, although less nutrients and more light in a shallower MLD favor smaller phytoplankton early in the growing seasons, intricacies of food wed suppress their relative abundance in the late spring and summer. This is likely because small phytoplankton, but not large phytoplankton, are a prey option for both zooplankton pools (*iv*, inset), and thus suffer disproportionately from an increase in the bulk zooplankton population. Again, there is no influence of temperature on loss rates because there are no temperature dependencies on any grazing or non-grazing loss terms. However, there is now a relatively large contribution from interaction effects, which also work to buffer the increase in loss rates and enhance the increase phytoplankton biomass. Large interaction effects loosely mirror the effects of community composition and may reflect the amplification of community composition effects by higher mean biomass.

1.3 OECO-v2 - Tropical Pacific

Unlike biomass in the light-limited Southern Ocean, in OECO-v2, the Tropical Pacific experiences a widespread bottom-up driven decrease in biomass (Supplementary Fig. 7c). Here a shallow MLD (*i*) exacerbates nutrient stress and decreases phytoplankton specific divisions rates by 11% (*ii*) despite more light and warmer water (*vi*). Worse growth conditions lead to 11% less phytoplankton (*iii*) and 24% less zooplankton biomass (*viii*). Reduced grazing pressure (*vii*) is driven by the reduction in grazers (*viii,v*, purple) and a reduction in grazing efficiency (*v*, green). As above, this acts as a stabilizing feedback, but here buffers a decline, rather than increase, in phytoplankton biomass.

However, working in the opposing direction, grazing pressure is increased through changes

in the vertical distribution (*v, x*, blue). Climate driven shoaling of the mixed layer leads to the formation of a deep biomass maxima (DBM), likely required to facilitated nutrient uptake (*iv* - inset). The formation of a DBM decreases the dilution length scale (*iv*), consolidating biomass which simultaneously exposes phytoplankton to more zooplankton and enables zooplankton to graze more efficiently (*ix*). Together, this facilitates a larger decrease in depth-integrated biomass than would occur in a well-mixed, uniform water column. Note, the change in clearance rates shown in *ix* is only with respect to changes in the vertical distribution ($\Delta\epsilon_{VD}$; 'see Methods'), rather than the full emergent state which is dominated by a decrease in bulk phytoplankton biomass driving a net decrease in clearance rates and grazing pressure. Interaction effects and changes in non-grazing losses play little role (*v, x*; black).

1.4 COBALTv2 - North Atlantic

Similarly, in COBALTv2, the North Atlantic experiences a widespread bottom-up dominated decrease in biomass (Supplementary Fig. 7d). Here, dramatically reduced deep winter mixing likely leads to an earlier exhaustion of new nutrients, reducing phytoplankton specific divisions rates throughout the growing season by 11% (*ii*). Again, worse growth conditions lead to a 21% and by 24% reduction in phytoplankton (*iii*) and zooplankton biomass (*viii*), respectively, followed by a stabilizing reduction in grazing pressure (*vii*).

However, here the role of other top-down controls on loss rates is more pronounced. First, unlike the models above, temperature dependent grazing rates contribute to an increase in grazing pressure (*v, x*, orange). Second, a nearly year-round shift toward smaller phytoplankton and zooplankton (*iv*) also contributes to a substantial increase in grazing pressure (*v, x*, teal) and non-grazing pressure (*v*, dashed teal). Grazing pressure increases because small zooplankton graze substantially faster than other classes of zooplankton but can only graze on small phytoplankton and bacteria (*iv*, inset; Supplementary Fig. 4). Non-grazing pressures increases

because only small phytoplankton are lost to a quadratic mortality term. Third, the dilution of biomass during the summer (*ix*) substantially decreases grazing pressure (*v*, blue line), providing as much of a buffering influences on phytoplankton biomass as the reduced zooplankton population (*v*; purple).

Note, unlike in OECO-v2's Tropical Pacific, the formation of DBM here has a diluting effect. Whether of not a DBM concentrates or dilution biomass depends on the steepness of the initial profile and protrusion of the DBM in the future profile. Similar to MEDUSA2.1's Southern Ocean, interactions effects plays a larger role, suggesting the introduction of more complex food-web, logically leads to an increased role for interaction effects. The net influence of these top-down controls at least partially cancels out (*v*).

1.5 PISCESv2.1 - Southern Ocean

In PISCESv2.1-IPSL, the Southern Ocean experiences a widespread decline in phytoplankton biomass which appears to be caused by dilution driven decoupling (Supplementary Fig. 8a). Here, there is a widespread 17% decrease in mean annual phytoplankton biomass (*iii*), despite a relatively large 26% increase in phytoplankton specific divisions rates (*ii*). A shoaling MLD leads to a 12% mean annual reduction in the dilution length scale (*iv*), which concentrates biomass toward the surface ocean (*iv* - inset). The redistribution of more concentrated of biomass leads to a 27% increase in clearance rates (*ix*) and is in turn the dominant driver (Δl_{VD}; *v,x*, blue) of a 28% increase in grazing pressure.

Temperature change (Δl_T) also makes a large contribution to increasing grazing pressure (*v,x*, orange) but is at least partially offset by increasing temperature dependent phytoplankton division rates and zooplankton mortality (Supplementary Fig. 4h). Finally, the contribution of decreasing zooplankton and phytoplankton biomass both work to reduce grazing pressure and limit the top-down change. Note, the scope of top-down control extends more broadly

across the Southern Ocean in PISCESv2-IPSL (Fig. 2h) but this regional sub-set was selected to illustrate more clearly where the contribution of vertical redistribution dominates all other terms, including temperature.

1.6 BFM5.2 - North Pacific

In BFM5.2, the North Pacific experiences a top-down decline in phytoplankton biomass, which appears to be caused by community composition driven decoupling (Supplementary Fig. 8b). Here, there is a widespread 32% decrease in mean annual phytoplankton biomass (*iii*), despite a 23% increase in phytoplankton specific divisions rates (*ii*). This is most pronounced during the spring bloom, in which phytoplankton biomass decreases by roughly half during the present-day peak in April. The initial decoupling between cell-growth and biomass appears driven by the first-order effect of shifts in community composition (Δl_{CC}; *v*, teal) and vertical distribution (Δl_{VD}; *v*, blue) during bloom initiation. Depressed biomass then appears to be sustained throughout the year via a 29% and 10% increase in relative abundance of small phytoplankton and small zooplankton, respectively. Since small zooplankton, which prefer small phytoplankton by a factor of 10, are parameterized to graze with a faster saturation grazing rate (3 vs. 2 d^{-1}) and much smaller half-saturation concentration (1.67 vs. 6.66 mmol m^{-3}) than large zooplankton, this allows the integrated zooplankton community to graze much more efficiency, with a 31% increase in clearance rates (*ix*), even as prey becomes substantially more scarce. In turn, the increase grazing efficiency allows grazing pressure to increase by 14% even as zooplankton biomass declines by 25%.

Increasing temperature also has a large positive first-order effect on the change in grazing pressure (*x*, orange); however, it is likely offset by a symmetric increase in nutrient-replete phytoplankton division rates and zooplankton mortality rates (Supplementary Fig. 4j), and thus not the driver of decoupling. Additionally, interaction effects have large negative first-order effect

on the change in grazing pressure (*x*, black); however, these work to reduce grazing pressure and thus increase phytoplankton biomass. The large negative interaction effect is likely explained by the fact the first order effect of temperature does not account for the large declines in zooplankton biomass, and thus over estimates its contributions. While shifts in vertical redistribution also work to reduce grazing pressure from May to November, their positive effect during bloom initiation likely plays an important role.

1.7 WOMBAT - Sub/Tropical Pacific

In WOMBAT, the Tropical Pacific experiences a top-down decline in phytoplankton biomass, which appears to be caused by temperature driven decoupling (Supplementary Fig. 8c). Here, there is a widespread 22% decrease in mean-annual phytoplankton biomass (*iii*), despite a 12% increase in phytoplankton specific divisions rates (*ii*). Unlike most models, the increase in phytoplankton specific loss rates here is driven by non-grazing pressure, rather than grazing pressure (*vii*). The increase in non-grazing pressure is clearly dominated by increasing temperature (*v*, dashed orange). Meanwhile, the influence of reduced phytoplankton (*iii*) and zooplankton biomass (*viii*) both work to reduce grazing and non-grazing pressure and stabilize the system.

Importantly, even though an identical temperature limitation term (1.066^T) is included on zooplankton mortality and nutrient-replete phytoplankton division rates (Supplementary Fig. 4c), these opposing influences of temperature on phytoplankton biomass do not appear to buffer the temperature-driven increases in loss rates to the same degree as in other models. This is explained by two reasons. First, in WOMBAT a further temperature dependency is included in the light limitation term, which exacerbates light limitation at higher temperatures. Since light and nutrients are not co-limiting in WOMBAT, this means the realized division rate saturates at high temperatures and low light levels. Low light levels can occur in the gyres because biomass predominantly accumulates in a deep biomass maxima. In turn, temperature has a dispropor-

tionate effect on loss rates over divisions rates. Second, the influence of temperature dependent zooplankton mortality is largely diminished by the fact that the temperature dependency on phytoplankton loss rates is included on a non-grazing (rather than grazing) term, which unlike for most models is the dominant loss term (Fig. 4). Combined with the fact there is low zooplankton biomass in the gyres to begin with, this means that temperature-driven increases in zooplankton mortality do have not have the same stabilizing influence on phytoplankton losses as they would if temperature-dependent grazing was simultaneously increase zooplankton growth.

While only part of the Tropical Pacific is under top-down control, almost all of the basin experiences a similarly large temperature-driven increase in non-grazing pressure (Fig. 5b) and decline in phytoplankton biomass (Fig. 2c). The difference is that in some cases exacerbated nutrient stress is large enough to also drive divisions rates down, meaning both bottom-up and top-down pressure drive biomass down, but the system remains classified as under bottom-up control.

1.8 CanOE - Sub/Tropical Atlantic

In CanOE, the Sub/Tropical Atlantic experiences a top-down increase in phytoplankton biomass, which appears to be caused by temperature driven decoupling (Supplementary Fig. 8d). Here, there is a widespread 8% increase in mean-annual phytoplankton biomass (*iii*), despite a -8% decrease in phytoplankton specific divisions rates (*ii*). This is clearly explained by a 31% decrease in grazing pressure (*vii*) that is driven by a 33% reduction in zooplankton biomass despite a 15% increase in zooplankton specific grazing rates (*ix*). The zooplankton population is able to decline despite grazing faster on a larger prey population due to an increase in their temperature-dependent morality rate (*iv*), which is not balanced by a temperature-dependent grazing rate. In turn the contribution of changes in the zooplankton population ($\Delta l_{\Sigma Z}$; *v,x*, purple) clearly dominate the change in loss rates.

This an example of insufficient predator self-limitation because predator mortality is not well coupled to predator biomass. Note, it is possible for other models to have temperature-dependent zooplankton mortality and sufficient predator self-limitation if they also include temperature-dependent zooplankton grazing. Since zooplankton biomass varies with ingestion rates, temperature effects are roughly balanced across predator growth and mortality, and thus do not impact the coupling between predator mortality rates are predator population size.

1.9 MEDUSA2.1 - North Atlantic

In MEDUSA2.1, the North Atlantic experiences a widespread bottom-up dominated decrease in biomass (Supplementary Fig. 9a). Here, dramatically reduced deep winter mixing likely leads to an earlier exhaustion of new nutrients, reducing phytoplankton specific divisions rates throughout the growing season by 34% (*ii*). Worse growth conditions lead to a 44% and by 59% reduction in phytoplankton (*iii*) and zooplankton biomass (*viii*), respectively, followed by a stabilizing reduction in grazing pressure (*vii*) driven by the reduce phytoplankton ($\Delta l_{\Sigma P}$; *v,x*, green) and zooplankton populations ($\Delta l_{\Sigma Z}$; *v,x*, purple).

Here, the bottom-up driven reduction in biomass is exacerbated by a top-down increase in grazing pressure driven by the shift in community composition (Δl_{CC}; *v,x*, teal) toward smaller phytoplankton and zooplankton (*iv*). Unlike COBALTv2, which simulates a similar bottom-up decline exacerbated by shifts in community composition (Supplementary Text 1.4), here the decline is unaffected by temperature but further exacerbated by vertical redistribution (Δl_{VD}; *v,x*, blue). This occurs in winter because MLD shoaling works to concentrate biomass. Similar to COBALTv2, throughout spring and summer, a reduction in the new nutrient supply works to dilute biomass into a deep biomass maxima below the previously highly concentrated surface expression (not shown). However, unlike in COBALTv2, this dilution works to increase grazing pressure rather than suppress it. That is because the baseline phytoplankton concentration is

mostly above the low prescribed half-saturation value for mesozooplankton grazing ($K_{1/2}$ = 1.99 mmol m^{-3}; Supplementary Fig. 4g). In turn, downward concavity above $K_{1/2}$ in the prescribed type III response function mean clearance rates increase as the prey concentration is reduced. The combined effect is a top-down driven increase in clearance rates (*ix*) during the spring and summer that exacerbates the bottom-up, nutrient driven decline.

1.10 PISCESv2 - North Atlantic

In PISCESv2-CNRM, the North Atlantic experiences a widespread top-down decrease in biomass cause by dilution driven decoupling (Supplementary Fig. 9b). Here, there is a widespread 31% decrease in mean annual phytoplankton biomass (*iii*), despite a relatively large 23% increase in phytoplankton specific divisions rates (*ii*). A shoaling MLD leads to a 19% mean-annual reduction in the dilution length scale (*iv*). Unlike COBALTv2, and MEDUASA2.1, the reduction in the overwinter nutrient supply does not lead to the formation of a DBM, such that reduced mixing works primarily to concentrate biomass toward the surface ocean, particularly in the winter (*iv* - inset). The redistribution of more concentrated of biomass in turn leads to a 24% increase in clearance rates (*ix*) and is clearly the dominant driver (Δl_{VD}; *v,x*, blue) of a 23% increase in grazing pressure. This is followed by a stabilizing reduction in grazing pressure (*vii*) driven by the reduced phytoplankton ($\Delta l_{\Sigma P}$; *v,x*, green) and zooplankton populations ($\Delta l_{\Sigma Z}$; *v,x*, purple).

1.11 BFM5.2 - North Atlantic

In BFM5.2, the North Atlantic experiences a top-down decline in phytoplankton biomass, which appears to be caused by community composition driven decoupling (Supplementary Fig. 9c). Here, there is a widespread 27% decrease in mean-annual phytoplankton biomass (*iii*), despite a 18% increase in phytoplankton specific divisions rates (*ii*). The drivers appear nearly identical to those simulated in the North Pacific (Supplementary Fig. 8b; Text 1.6), but with an

even larger contribution from shifts in community composition to grazing pressure ($\Delta l_{g,CC}$; *v,x*, teal). Here, there is 24% and 17% increase in relative abundance of small phytoplankton and small zooplankton, respectively, and the mean-annual contribution of $\Delta l_{g,CC}$ exceeds all other terms, including temperature (*x*). Again, the strong effect of shifting community composition in BFM5.2 is associated with the strong prescribed increase in grazing rates for small zooplankton grazing on small phytoplankton. For example, small zooplankton can graze 10 times faster on small phytoplankton than large zooplankton on large phytoplankton at a fixed prey concentration of 1 mmol m^{-3} (Supplementary Fig. 4j).

1.12 MARBL - North Atlantic

In MARBL, the North Atlantic experiences a large top-down decline in phytoplankton biomass, which appears to be caused by stability driven (re)coupling (Supplementary Fig. 9d). Here, there is a widespread 52% decrease in mean annual phytoplankton biomass (*iii*), despite a 18% increase in phytoplankton specific divisions rates (*ii*). The reduction in phytoplankton biomass increases to 70% at its May-peak, essentially shutting down the North Atlantic Spring bloom. Unlike other models which simulate the suppression of the North Atlantic spring bloom, here it is clearly not driven from the bottom-up (as in COBALTv2 and MESDUSA2.1), via reduced spring-time dilution (as in PISCESv2-CNRM) or via shifting community composition (as in BFM5.2). This is evident from the fact that divisions rates increase and the contribution of redistribution (Δl_{VD}; *v,x*, blue) and community composition (Δl_{CC}; *v,x*, teal) to loss rates is minor. Moreover, during the spring-bloom Δl_{VD} works to relieve grazing pressure via dilution into a DBM (*iv*).

Instead, the only driver that can explain the 38% increase in grazing pressure (*vii*) is the massive contribution of changes in the size of the phytoplankton population which increase substantially during the blooming period ($\Delta l_{\Sigma P}$; *v,x*, green). The 0.3 d^{-1} June contribution of

$\Delta l_{\Sigma P}$ in the MARBL-simualted North Atlantic is over 30 times larger the the global ensemble mean. Unlike most models which include upward concavity in their grazing formulation, MARBL prescribes a very steep (low $K_{1/2}$) type II response. This causes clearance rates to increase extremely rapidly as prey biomass declines. This destabilizing property can work to accelerate large blooms as it makes zooplankton less efficient grazers as their prey concentrations increase, leading to large decoupling periods over which biomass can accumulate before zooplankton population gains and nutrient depletion allow loss processes to catch up.

This phenomena appears most prolific in the North Atlantic (Fig. 5c) because a) canonical bottom-up controls on the spring bloom help open the decoupling window and b) because deep winter mixing dilutes the spring-time phytoplankton seed population, which increases the destabilizing properties of the functional response. Since the type II response saturates, strong downward curvature at low prey populations leads to larger reductions in clearance rates as low (compared to high) prey concentrators increase. This means that highly diluted phytoplankton, stimulated with a rush of nutrient and light, are able to rapidly outpace the zooplankton population which suffers from dramatic reductions in grazing efficiency as the phytoplankton bloom initiates.

We in turn believe the shutdown of the MARBL-simulated North Atlantic spring bloom is related to the reduced dilution of over-wintering seed phytoplankton related to the 300+ m shoaling of the winter MLD. This is supported by the reduction in the winter/early spring dilution length scale (*iv*) and the increase in the winter/early spring stabilizing influence of the grazing formulation (*ix*, see 'Methods').

Supplemental Figures

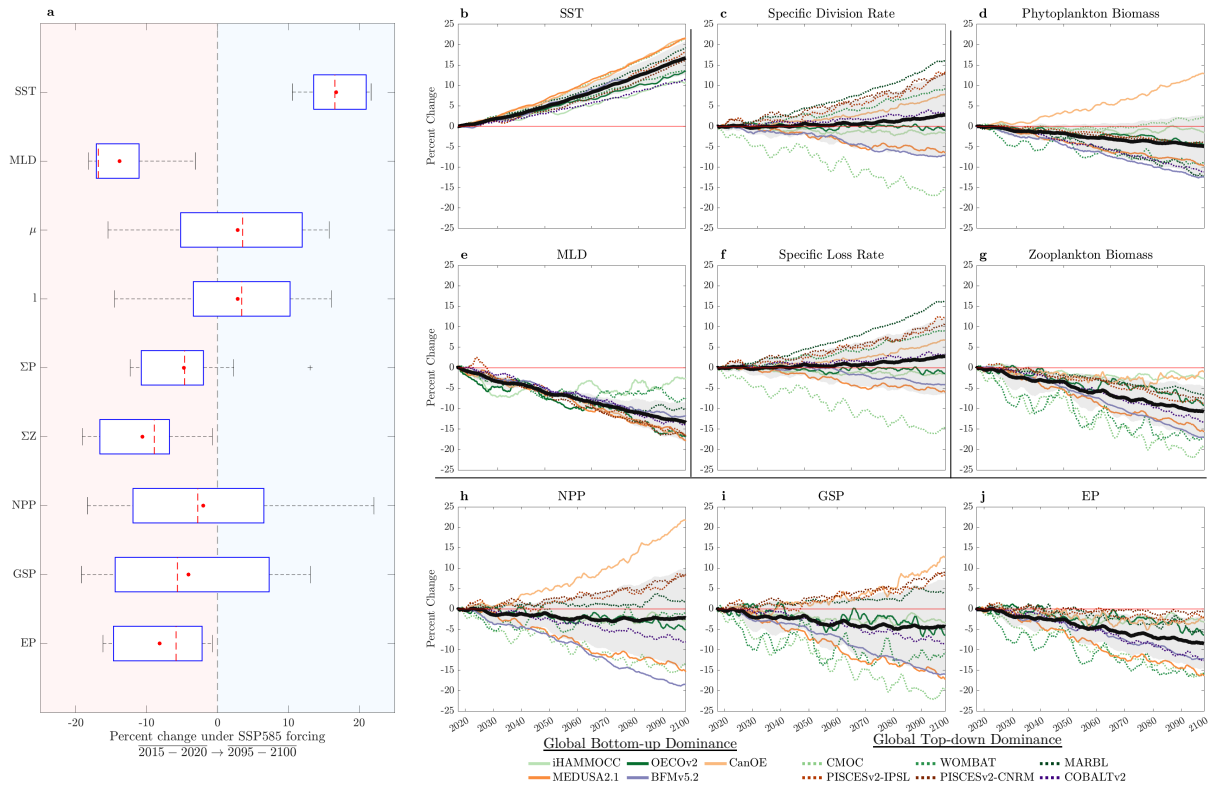

Figure S1: Evolution of physics and biogeochemistry in CMIP6 models in high emissions scenario (SSP585). **a** Box plots and **b-j** time series for relative change (%) in sea surface temperature (SST), mixed layer depth (MLD), phytoplankton specific division rates (μ), phytoplankton specific loss rates (l), depth-integrated phytoplankton biomass (ΣP), depth-integrated zooplankton biomass (ΣZ), net primary production (NPP), gross secondary production (GSP) and export production through 100 m (EP). All variables are area and biomass weighted in space and time (see 'Methods'). Box and whisker plots show median (dashed red line), mean (red dot), interquartile range (IQR; blue box), and 1.5 times the IQR (whiskers). Times series are 12 month moving means.

	BGC Model	Earth System Model	Exp. ID (SSP585)	Institution (Location)	Output variables required to diagnostically compute loss terms																				
					Phytoplankton					Zooplankton			Other OM		Physics		Nutrient Limitation				Division rate			
					phyc	pico	diaz	diat	misc	zooc	micro	meso	detoc	bacc	thetao	MLD	N	Fe	P	Si	pico	diat	diaz	misc
	iHAMOCC (113)	NorESM2-LM (113)	r1i1p1f1 (128)	NCC (NOR)	g, ng					g														
	CMOC (123)	CanESM5 (114)	r1i1p2f1 (129)	CCCM (CAN)	g, ng					g														
	WOMBAT (115)	ACCESS ESM1.5 (115)	r1i1p1f1 (130)	CSIRO (CAN)	g, ng					g					ng									
	OECO-v2 (116)	MIROC-ES2L (116)	r1i1p1f2 (131)	JAMSTEC (JAP)	g, ng			g		g														
	MARBL (124)	CESM2 (117)	r10i1p1f1 (132)	NCAR (USA)		g, ng	g, ng	g, ng		g					g, ng									
	CanOE (118)	CanESM5-CanOE (118)	r1i1p2f1 (133)	ECCC (CAN)			g, ng		g, ng		g	g												
	MEDUSA2.1 (119)	UKESM1-0-LL (119)	r1i1p1f2 (134)	Met Office, NERC (UK)			g, ng		g, ng		g	g												
	PISCESv2 (125)	IPSL-CM6A-LR (119)	r1i1p1f1 (135)	IPSL (FR)			g, ng		g, ng		g	g	g		g	ng	ng	ng	ng	ng				
	PISCESv2 (125)	CNRM-ESM2.1 (120)	r1i1p1f2 (136)	CNMR (FR)			g, ng		g, ng		g	g	g		g	ng	ng	ng	ng	ng				
	BFM5.2 (127)	CMCC-ESM2 (121)	r1i1p1f1 (137)	CMCC (ITA)			g, ng		g, ng		g	g		g	g		ng	ng	ng	ng				
	COBALTv2 (126)	GFDL-ESM4.1 (122)	r1i1p1f1 (138)	GFDL (USA)		g, ng	g, ng	g, ng	g, ng		g	g		g	g, ng						ng	ng	ng	ng

Fully Available | Minor Assumptions | Major Assumptions

'g': Required to compute grazing losses
'ng': Required to compute grazing losses

Figure S2: Description of models reviewed and diagnostics required. References are provided for all biogeochemical models, Earth system models and specific ensemble members relating to each simulation examined. On the right a list of all model output required to diagnostically compute loss terms. Output highlighted in yellow or orange were incomplete and required additional minor or major assumptions, respectively (see 'Methods').

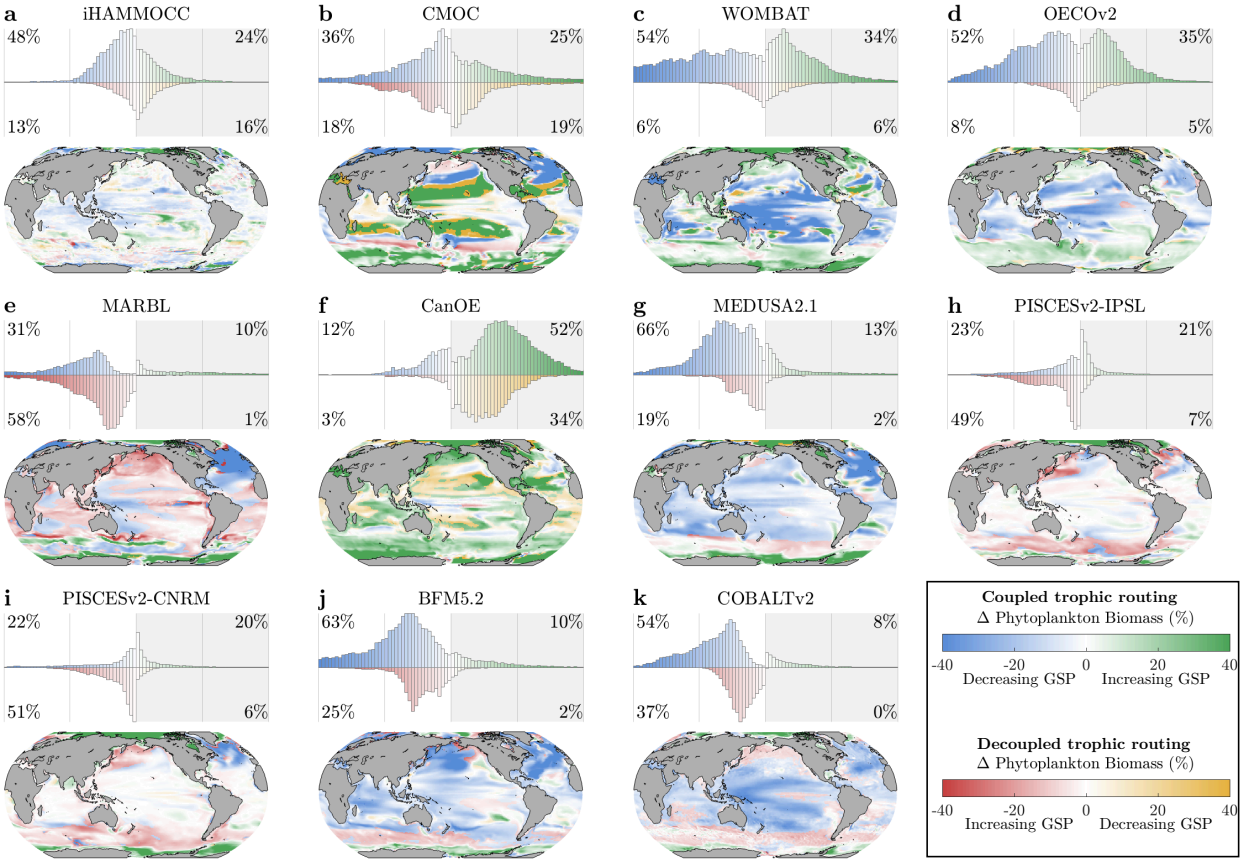

Figure S3: Decoupling between changes in biomass and Gross Secondary Production (GSP) As per Figure 2, but partitioning is determined based on whether phytoplankton biomass and GSP (rather than divisions rates) move in the same direction. Regions where they diverge are plotted on a red-yellow color-bar in the global maps and the bottom of the phytoplankton biomass change histograms.

	BGC Model; ESM	Phytoplankton Group and Relative Loss Rates Grazing | Non-Grazing	Grazing Losses	Non-Grazing Losses	Temperature Limitation (L^T) Phyto Loss	Phyto Growth	Zoo Loss
a	iHAMOCC NorESM2-LM	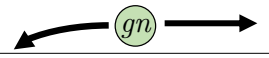	$1.2\frac{P^*}{9.78+P^*}\mathrm{Z}$	$.04P^*$	-	1.066^T	-
b	CMOC; CanESM5		$0.85\frac{P^2}{1.33^2+P^2}\mathrm{Z}$	$.05P + .015P^2$	-	Arrhenius $T_r = 30$	Arrhenius $T_r = 30$
c	WOMBAT; ACCESS ESM1.5	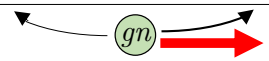	$1.58\frac{P^2}{6.57^2+P^2}\mathrm{Z}$	$.039L^TP + .038P^2$	1.066^T	1.066^T	1.066^T
d	OECO-v2; MIROC-ES2L	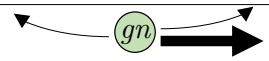	$2\frac{P^2}{9.37^2+P^2}\mathrm{Z}$	$.05P + .0075P^2$	-	$e^{(T/15.65)}$	-
		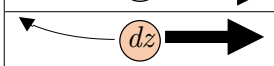	$2\frac{P^2}{9.37^2+P^2}\mathrm{Z}$	$.025P$			
e	MARBL; CESM2	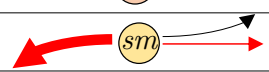	$3.3L^T\frac{P^*}{1.2+P^*}Z$	$.1L^TP^* + .01P^{*1.75}$	$1.7^{\frac{T-30}{10}}$	$1.7^{\frac{T-30}{10}}$	$1.7^{\frac{T-30}{10}}$
		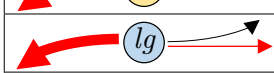	$3.3L^T\frac{P^*}{1.2+P^*}Z$	$.1L^TP^* + .01P^{*1.75}$			
		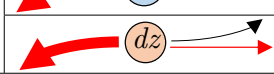	$3.15L^T\frac{P^*}{1.2+P^*}Z$	$.1L^TP^* + .01P^{*1.75}$			
f	CanOE; CanESM5-CanOE	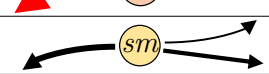	$1.7(1-e^{-.25P})Z_{sm}$	$.05P + .06P^2$	-	Arrhenius $T_r = 25$	Arrhenius $T_r = 25$
		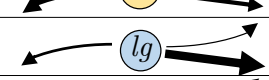	$.85(1-e^{-.25P_\Sigma})Z_{md}\left(\frac{P}{P_\Sigma}\right)$	$.1P + .06P^2$			
g	MEDUSA2.1; UKESM1-0-LL	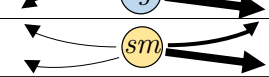	$2\frac{.75P^2}{5.3^2+P_\Sigma^2}Z_{sm} + .5\frac{.15P^2}{1.99^2+P_\Sigma^2}Z_{md}$	$.02P + .1\frac{P}{3.31+P}P$	-	1.066^T	-
		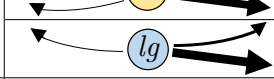	$.5\frac{.35P^2}{1.99^2+P_\Sigma^2}Z_{md}$	$.02P + .1\frac{P}{3.31+P}P$			
h i	PISCESv2; IPSL-CM6a-LR & CNRM-ESM2.1	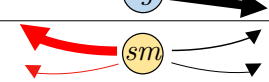	$3L^TF\frac{P^*}{20+P_\Sigma}Z_{sm} + .75L^TF\frac{.3P^*}{20+P_\Sigma}Z_{md}$	$.01\frac{P}{.2+P}P + .03f(\mathrm{mld})P^2$	1.079^T	1.066^T	1.066^T
		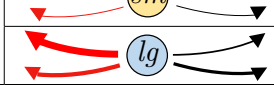	$3L^TF\frac{.1P^*}{20+P_\Sigma}Z_{sm} + .75L^TF\frac{P^*}{20+P_\Sigma}Z_{md}$	$.01\frac{P}{.2+P}P + .03f(\mathrm{mld}, L^N)P^2$			
j	BFM5.2; CMCC-ESM2	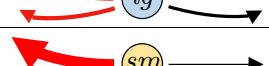	$3L^T\frac{\left(\frac{P}{1.67+P}\right)P}{1.67+P_\Sigma}Z_{sm}$	$.05\frac{.1}{.1+(L^N)}P$	$2^{\frac{T-10}{10}}$	$2^{\frac{T-10}{10}}$	$2^{\frac{T-10}{10}}$
			$3L^T\frac{\left(\frac{.1P}{1.67+P}\right)P}{1.67+P_\Sigma}Z_{sm} + 2L^T\frac{P}{6.66+P_\Sigma}Z_{md}$	$.05\frac{.15}{.15+(L^N)}P$			
k	COBALTv2; GFDL-ESM4.1	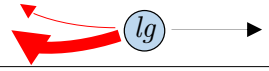	$1.28L^T\frac{\left(\frac{P}{\sqrt{P_\Sigma^2}}\right)P}{8.28+P_\Sigma}Z_{sm}$	$.03\ L^TP^2 + .015f(\mu, L^T)P^2$	$e^{.063T}$	$e^{.063T}$	$e^{.063T}$
			$.57L^T\frac{\left(\frac{P}{\sqrt{P_\Sigma^2}}\right)P}{8.28+P_\Sigma}Z_{md} + .23L^T\frac{\left(\frac{P}{\sqrt{P_\Sigma^2}}\right)P}{8.28+P_\Sigma}Z_{lg}$	$.45f(\mu, L^T)P^2$			
		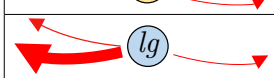	$.57L^T\frac{\left(\frac{P}{\sqrt{P_\Sigma^2}}\right)P}{8.28+P_\Sigma}Z_{md} + .23L^T\frac{\left(\frac{P}{\sqrt{P_\Sigma^2}}\right)P}{8.28+P_\Sigma}Z_{lg}$	-			

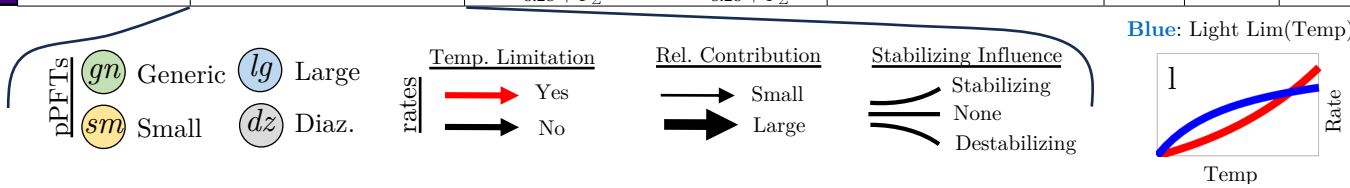

Figure S4: Formulation of loss terms in CMIP6 models. Loss process schematic arrows are scaled to the relative contribution of each term evaluated at the inter-model median plankton concentration/SST. The color/inflection of arrows indicate their temperature sensitivity and predominant stabilizing influence on population dynamics, respectively (see 'Methods'). Variables P, P^*, and P_Σ refer to the class-specific phytoplankton concentration, P with a small threshold removed, and the integrated prey concentration (inclusive of non-phytoplankton prey). Z_i refers to the class-specific zooplankton concentration. Temperature limitation terms (L_T) are defined on the right. Models in which temperature increases maximum phytoplankton growth rates *and* exacerbates light limitation are colored blue. Functional dependencies on nutrient limitation (L_N), mixed layer depth (mld) and division rates (μ) are included explicitly in diagnostics but abbreviated here. Exudation and/or autotrophic respiration terms explicitly computed in iHAMMOCC, CanOE, BFM5.2 and COBALTv2 are not considered here as they would be implicitly included in NPP in other models (see 'Methods'). PISCESv2 includes a global prey limitation term (F) that reduces grazing when P_Σ is low.

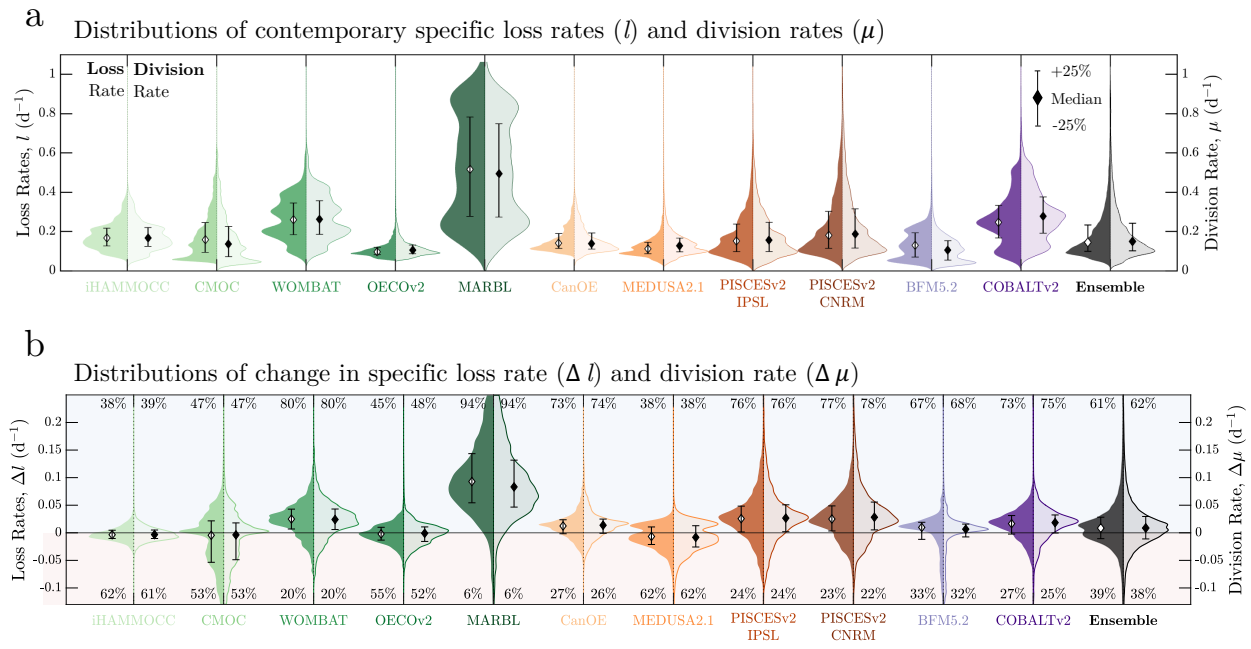

Figure S5: Balance of growth and loss rates. **a** Distributions of contemporary specific loss rates (left violin plots) and specific division rates (left violin plots) for each model. **a** Distributions of 21st century change in specific loss rates (left violin plots) and specific division rates (left violin plots) for each model. Annotations specify positive and negative fractions of distribution. All distributions are depth-integrated and biomass and area weighted (see ‘ Methods’).

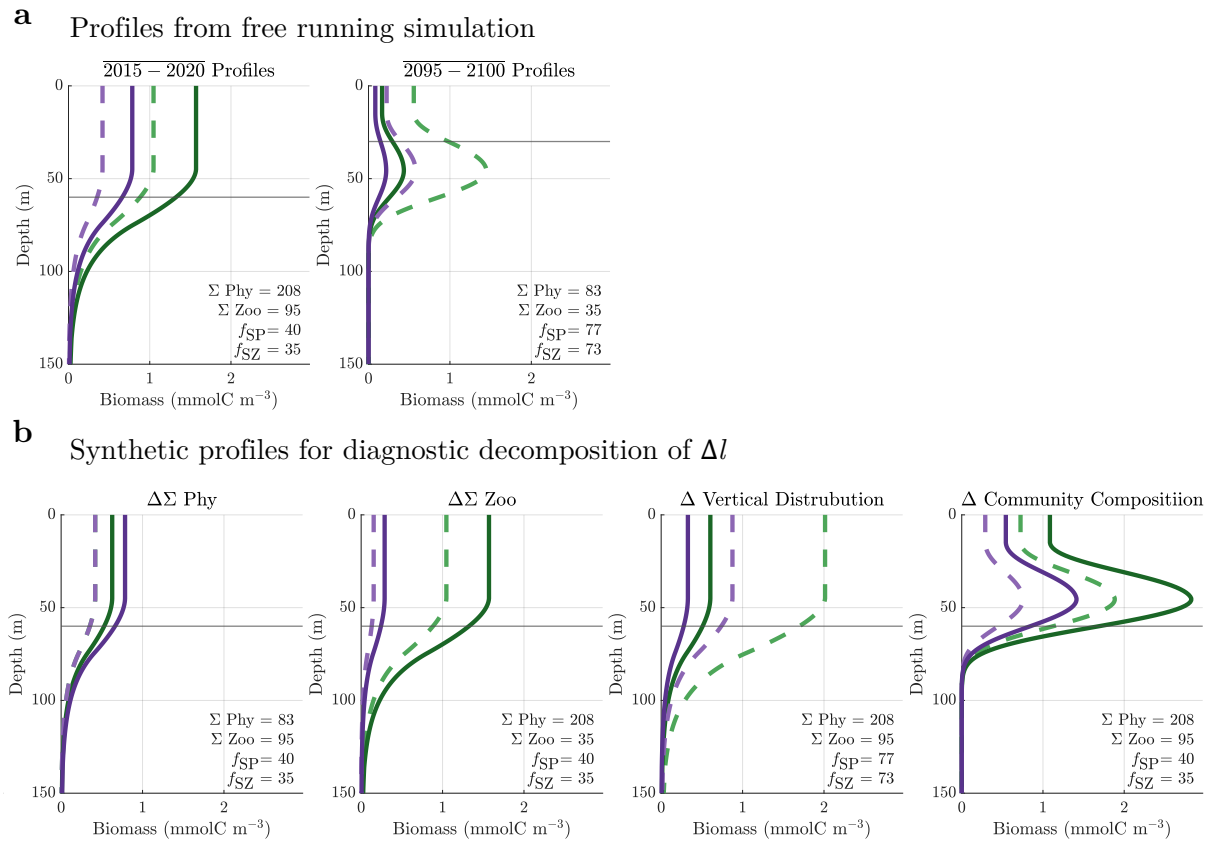

Figure S6: Schematic of idealized profiles to illustrate how the loss rate decomposition is computed. **a**) Idealized phytoplankton and zooplankton profiles are shown from $\overline{2015-2020}$ and $\overline{2095-2100}$. **b**) Four synthetic profiles are created by conserving all but one property of the $\overline{2015-2020}$ climatological profiles, but allowing a single property to evolve with the free-running $\overline{2095-2100}$ profiles. Depth-integrated phytoplankton biomass (ΣPhy), zooplankton biomass (ΣZoo), and the fraction of small phytoplankton (f_{SP}) and zooplankton (f_{SZ}) are shown for each profile to illustrate where they are conserved. Depth-integrated, biomass weighted, phytoplankton specific loss rates are subsequently compute on each synthetic profile to estimate the isolated impact of the that property on the evolution of phytoplankton specific loss rates. Synthetic profiles for the change in temperature are not shown. Synthetic profiles are computed at monthly resolution, conserving the relevant properties of the 5-year climatology from $\overline{2015-2020}$ for each month.

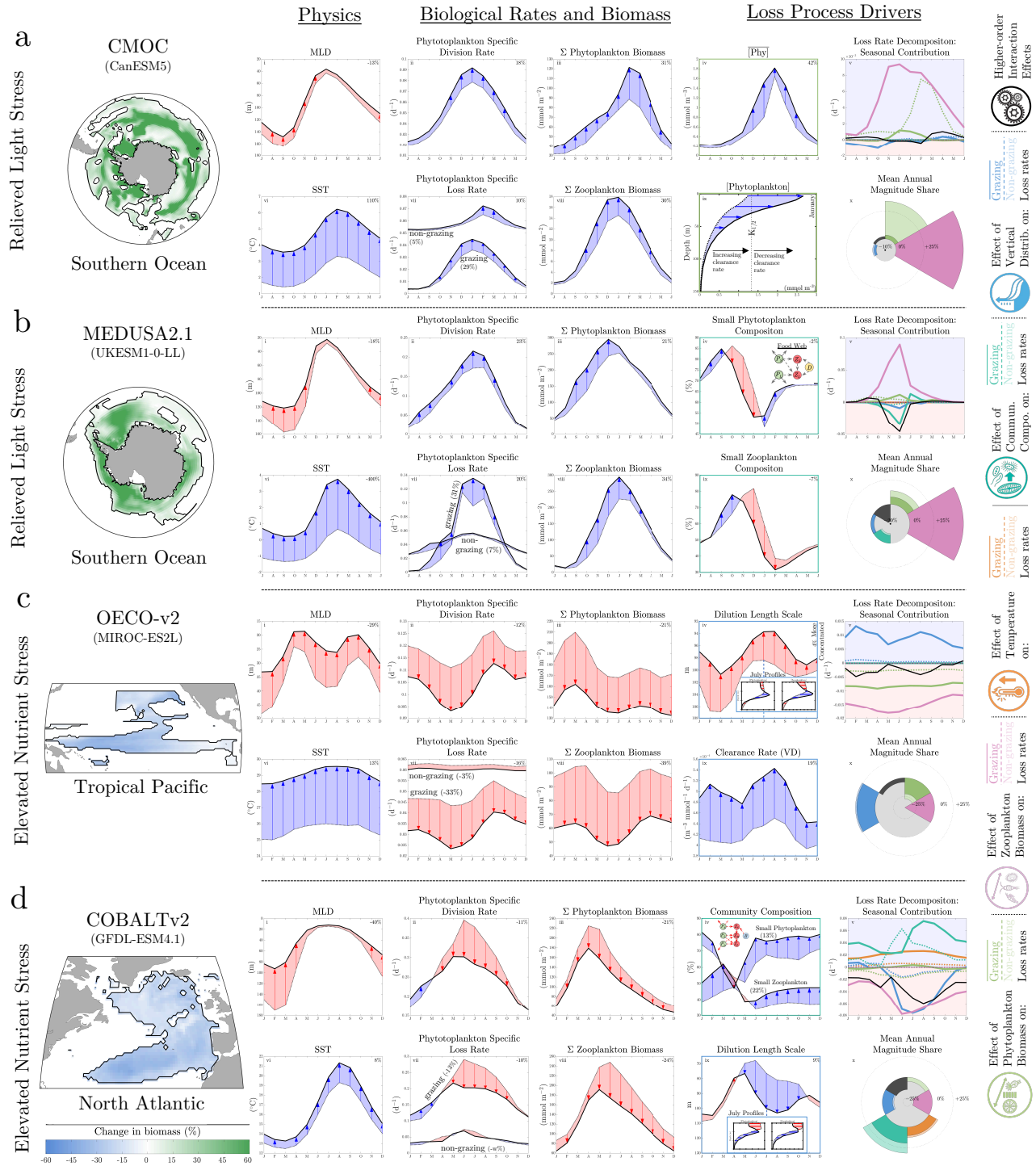

Figure S7: Case studies for bottom-up control. Four models exhibiting regional bottom-up driven biomass **a, b)** increase and **c, d)** decrease. Regional distributions of $\Delta\Sigma$Phy are shown on the left. Regional boundaries were selected for illustrative purposes by filtering for increasing/decreasing biomass under bottom-up/top-down control within a specified Longhurst province. Middle panels (i-iv,vi-ix) show the $\overline{2010-2015}$ (dashed) and $\overline{2095-2100}$ (solid) climatologies for specified variables. Panel v shows change (Δ) for each loss term. Legend on right. Panel x shows the magnitude share for the mean annual contribution of each term to Δl (see 'Methods'). Colored boarders indicate panels which help explain the change in the associated loss term. Case studies are described in detail in Supplementary Text 1.1-1.4

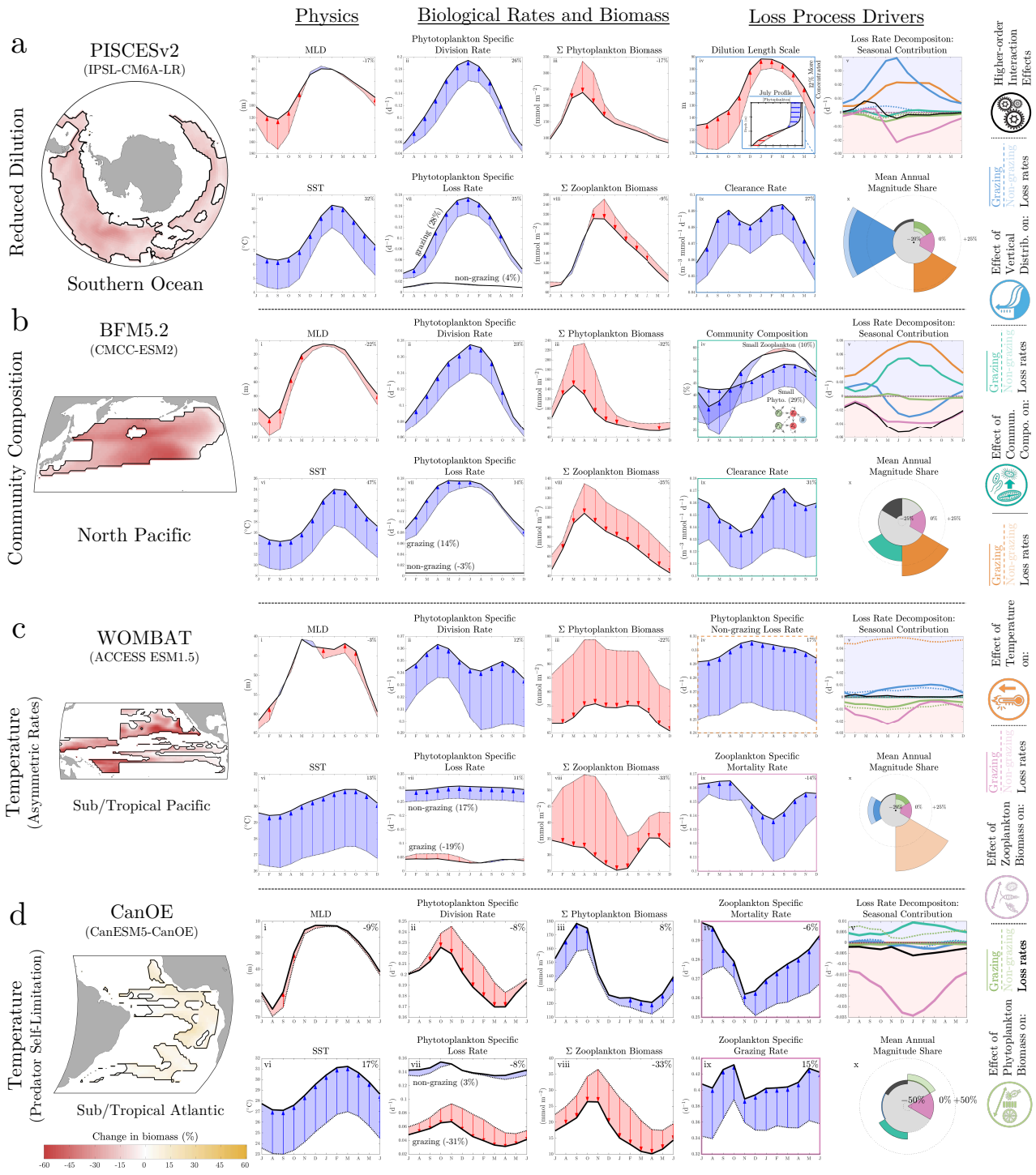

Figure S8: Case studies for top-down control. As per Supplementary Fig. 7. Four different regions from four different models are selected to illustrate how phytoplankton biomass can decrease despite elevated division rates via **a)** dilution driven decoupling **b)** community composition driven decoupling, **c)** temperature driven via asymmetric temperature-dependent growth and loss rates and **d)** temperature driven decoupling via insufficient predator self-limitation. Case studies are described in detail in Supplementary Text 1.5-1.8

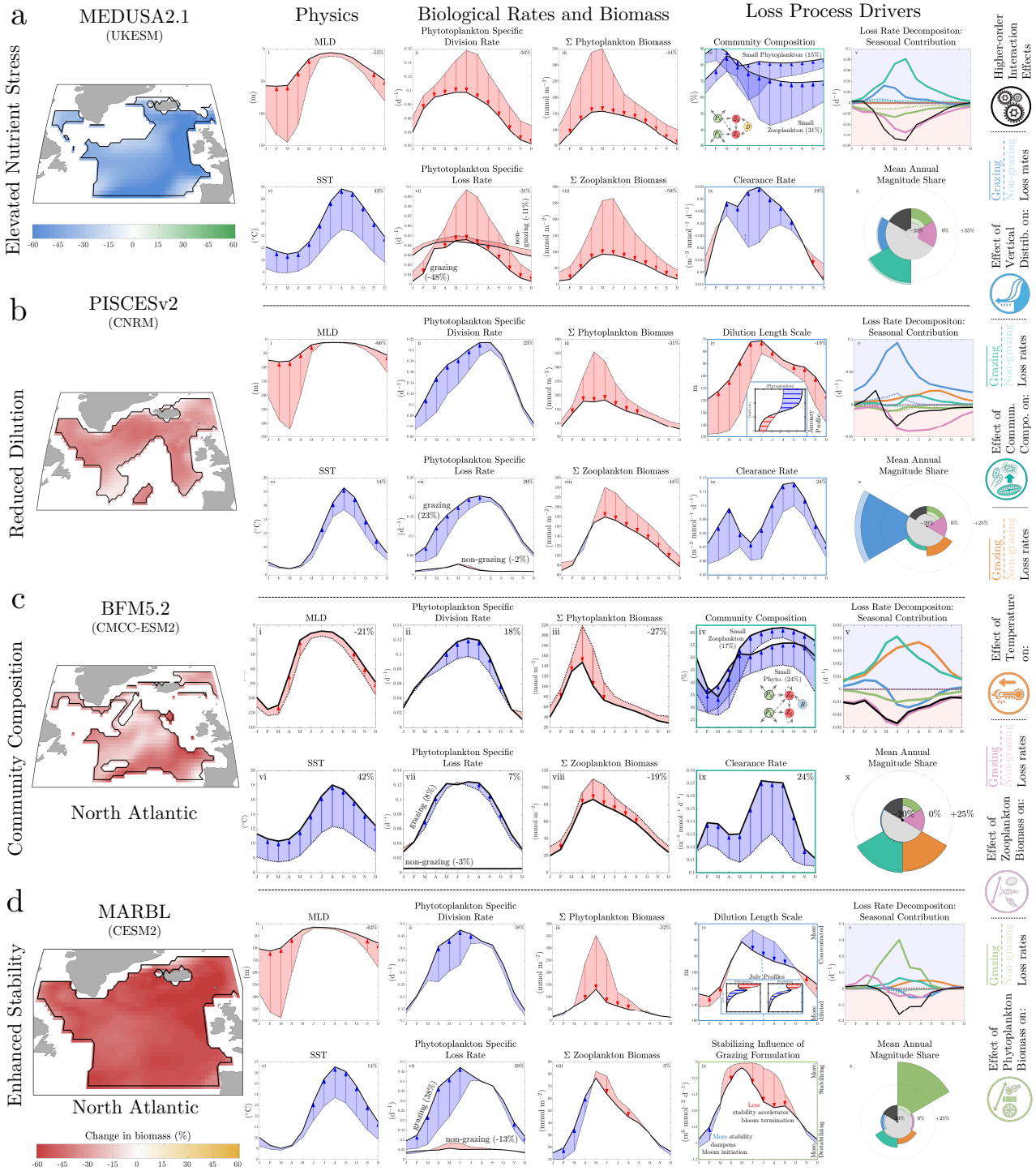

Figure S9: Case studies for North Atlantic biomass declines. As per Supplementary Fig. 7. Four different models are selected to illustrate how phytoplankton biomass can decrease in the North Atlantic through fundamentally different mechanisms, including **a)** bottom-up nutrient stress **b)** dilution driven decoupling, **c)** community composition driven and **d)** stability driven (re)decoupling. Case studies are described in detail in Supplementary Text 1.9-1.12

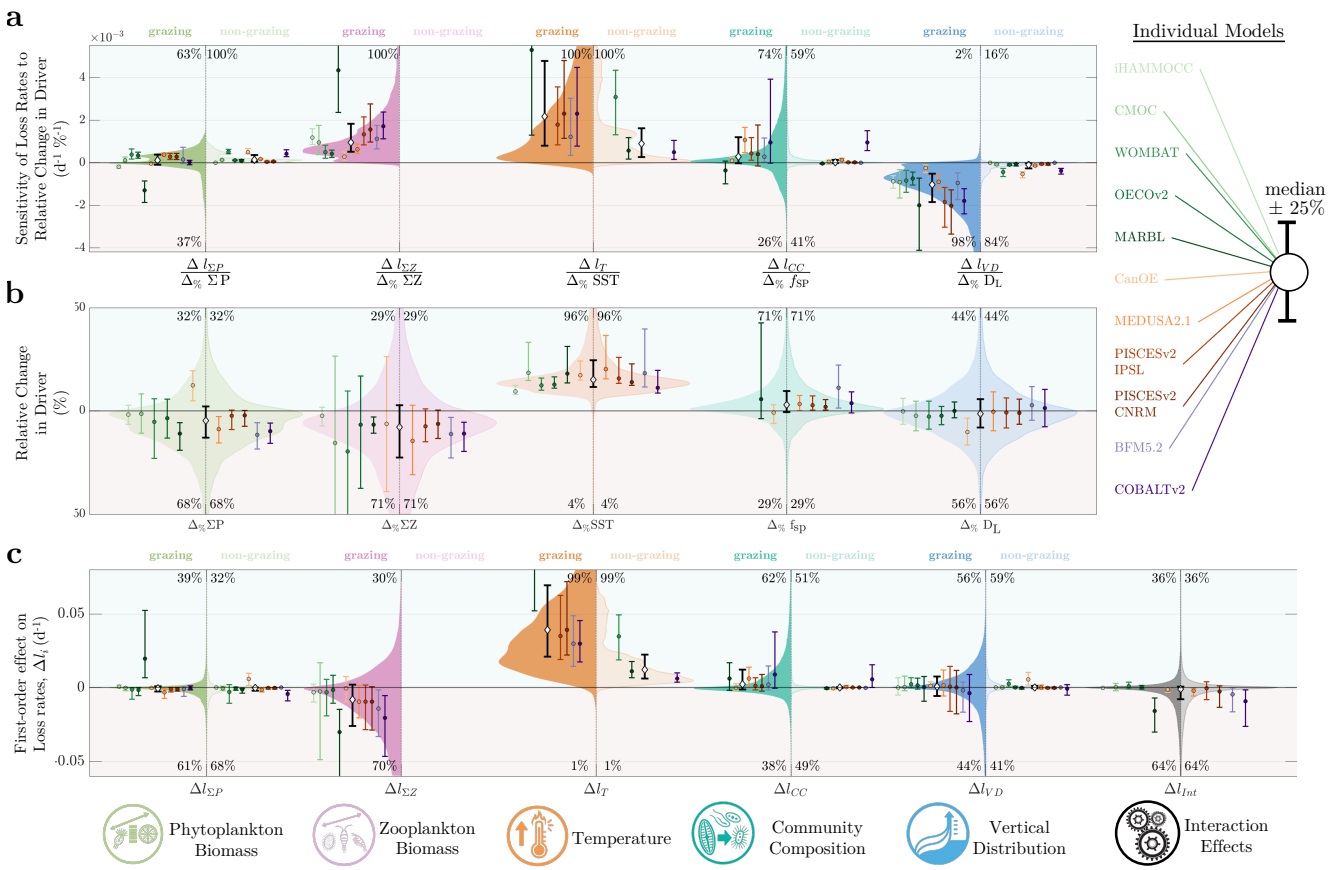

Figure S10: Sensitivity of loss rates to environmental change. **a** The sensitivity of loss rates to the isolated relative change in phytoplankton biomass, zooplankton biomass, temperature, community composition and vertical distribution (d^{-1} $\%^{-1}$) is computed by dividing **b** the relative change in each forcing ($\%$) into **c** the first order effect of each driver on loss rates (d^{-1}). See 'Methods' for details. Ensemble (violin plots) and individual models (box-whisker) are shown. **a** and **c** are split into grazing (left) and non-grazing (right) terms. Annotations specify positive and negative fractions of distribution. Interaction effects shown in **c** are not sensitive to a specific driver.

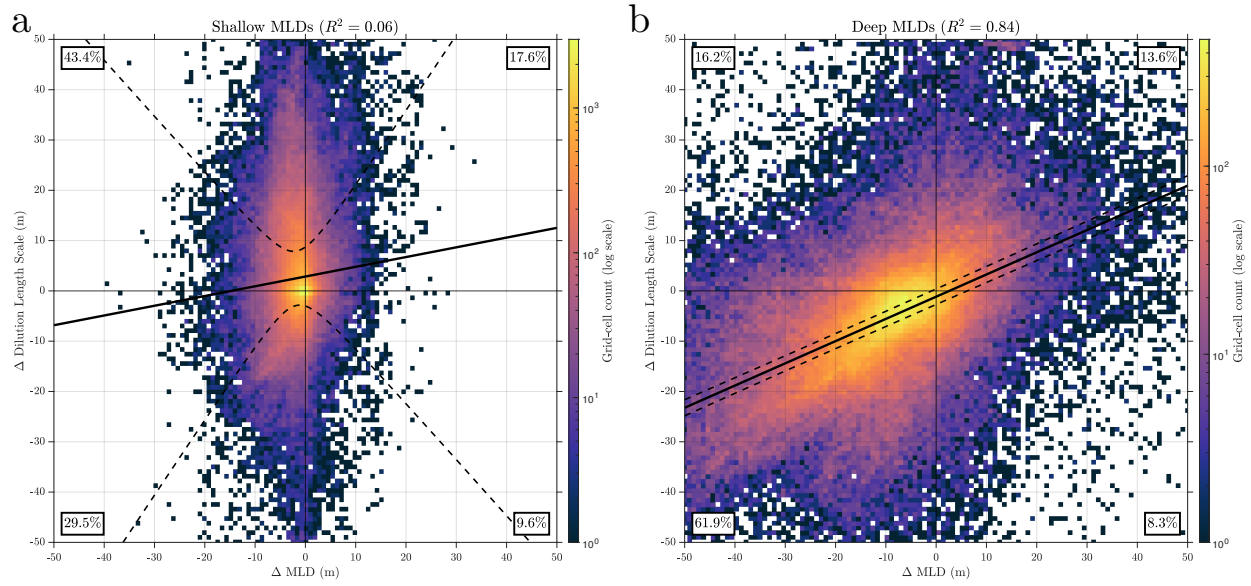

Figure S11: Relationship between MLD shoaling and dilution of biomass. **a)** When climate-modified MLDs start from a shallow contemporary MLD ($\overline{\text{MLD}_{2015-2020}}$ <30m), there is no relationship between the direction and magnitude of MLD change and the dilution or concentration of phytoplankton and zooplankton populations, as quantified by the Dilution Length Scale (see 'Methods'). This is due to the emergence and/or modification of deep biomass maxima below shallow MLDs, which can both decrease or increase D_L depending on the shape of the initial and final profiles. See descriptions of case studies for OECO-v2 Tropical Pacific (Supplementary Text 1.3/Fig. 7c) vs COBALTv2 North Atlantic (Supplementary Text 1.4/Fig. 7d) for examples of how a DBM can consolidate and dilute biomass, respectively. **b)** When climate-modified MLDs start from a deep contemporary MLD ($\overline{\text{MLD}_{2015-2020}}$ >50m), there is a strong relationship between the direction and magnitude of MLD change and the dilution or concentration of phytoplankton and zooplankton populations. This is because shoaling is more likely to more homogeneously concentrate biomass in a smaller volume of water when surface nutrients are more abundant. The percent of biomass in each quadrant is annotated. Scatter plots include all models.

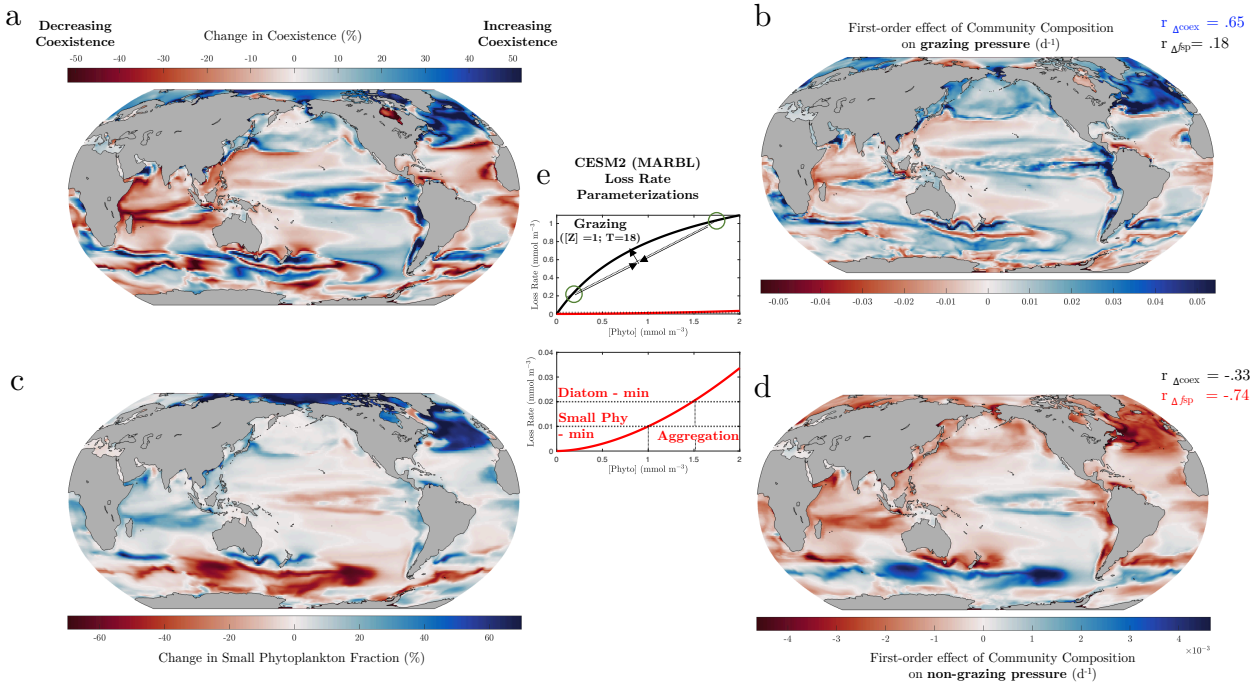

Figure S12: Coexistence driven change in $\Delta l_{g,\mathrm{CC}}$ in MARBL. In MARBL, **a**) The change in coexistence between small phytoplankton and diatoms is positively well correlated (r=.65) with **b**) the effect of changes in community composition on grazing pressure ($\Delta l_{g,\mathrm{CC}}$). Whereas, **c**) the change in the fraction of of small phytoplankton (f_{sp}) is negatively well correlated (r=-.33) with **c**) the change in non-grazing pressure ($\Delta l_{ng,\mathrm{CC}}$). **e**) Increasing coexistence increases $\Delta l_{g,\mathrm{CC}}$ through non-nonlinearities in the steeply downwardly concave (very low $K_{1/2}$) functional response. Increasing f_{sp} decreases $\Delta l_{ng,\mathrm{CC}}$ due to a lower minimum aggregation rate for small phytoplankton. Coexistence is computed as the absolute value of the difference between the fraction of small phytoplankton and diatoms, such that small number values reflect more similarly sized populations (see 'Methods'). Note, however, the sign in **a**) is reversed for more intuitive sign-notation. All plots show the mean change between $\overline{2015-2020}$ and $\overline{2095-2100}$.